

# Structure and Transport Characteristics of Single-Crystal and Ceramic $\text{ZrO}_2\text{--Y}_2\text{O}_3$ Solid Electrolytes<sup>1</sup>

E. E. Lomonova<sup>a</sup>, D. A. Agarkov<sup>b,c</sup>, M. A. Borik<sup>a</sup>, G. M. Korableva<sup>b</sup>, A. V. Kulebyakin<sup>a</sup>, I. E. Kuritsyna<sup>b</sup>, M. N. Mayakova<sup>a</sup>, F. O. Milovich<sup>a,d</sup>, V. A. Myzina<sup>a</sup>, N. Yu. Tabachkova<sup>a,d,\*</sup>, and E. I. Chernov<sup>e</sup>

<sup>a</sup> Prokhorov General Physics Institute, Russian Academy of Sciences, Moscow, Russia

<sup>b</sup> Institute of Solid-State Physics, Russian Academy of Sciences, Chernogolovka, Moscow oblast, Russia

<sup>c</sup> Moscow Physicotechnical Institute, Dolgoprudnyi, Moscow oblast, Russia

<sup>d</sup> National Research Technological University MISiS, Moscow, Russia

<sup>e</sup> Research and Production Enterprise EKON, Obninsk, Kaluzhskaya oblast, Russia

\*e-mail: ntabachkova@gmail.com

Received November 20, 2020; revised August 21, 2021; accepted August 31, 2021

**Abstract**—Directionally solidified single crystals of  $(\text{ZrO}_2)_{1-x}(\text{Y}_2\text{O}_3)_x$  solid solutions ( $x = 0.08\text{--}0.12$ ) are grown. The effect of the concentration of the stabilizing yttrium oxide on the transport characteristics of the  $\text{ZrO}_2$ -based single-crystal solid solutions is studied. In the studied composition range, it is the  $(\text{ZrO}_2)_{0.91}(\text{Y}_2\text{O}_3)_{0.09}$  crystal that has the maximal electrical conductivity. This crystal was milled, the resulting powder was used as a starting material for the manufacturing of ceramic samples by slip casting onto a moving substrate. The grains of the ceramic samples are sized 10–30  $\mu\text{m}$ ; the material density is 5.86  $\text{g}/\text{cm}^3$ . A comparative analysis of the structure and electrophysical properties of ceramic and single-crystal samples of the  $(\text{ZrO}_2)_{0.91}(\text{Y}_2\text{O}_3)_{0.09}$  solid electrolytes is carried out. The described method of the ceramic sample preparation is shown not leading to changes in their phase composition and crystal structure. The ionic conductivity of the single crystals and ceramics in the 973–1173 K temperature range were close to each other; at a temperature of 1173 K, their conductivity values are 0.076 and 0.065 S/cm, respectively.

**Keywords:** solid electrolytes, zirconia, single crystals, phase composition, structure, ionic conductivity

**DOI:** 10.1134/S1023193522020069

## INTRODUCTION

Zirconia-based materials are solid electrolytes; they are widely used in oxygen sensors for different media, oxygen pumps, and solid oxide fuel cells [1–6]. The demands placed on the materials are: high ionic conductivity and stability of characteristics at the operational temperatures, in conjunction with chemical inertness both in oxidative and reductive atmospheres. The manufacturing technology of the materials must provide for the possibility of obtaining mechanically strong and dense membranes of small thickness and large surface area, as well as shaped objects. Most commonly, such devices are based on polycrystalline materials. The ceramic technology practically is not constrained in the manufacturing of differently shaped and sized objects. It is well known, however, that the conductivity of the zirconia-based ceramic solid electrolytes may differ significantly depending on their manufacturing methods [7–24].

The reason thereof may be difference in the material's microstructure, impurity content, and thermal pre-history connected with the method of its preparation.

The microstructure dependence of the conductivity is caused by a difference in the properties of the grain bulk and intergrain space (the intergrain boundaries) [7–14, 18–45], as well as their ratio in the material's structure. In addition, materials can contain pores and impurity-dopants favoring their better sintering. In  $\text{Zr}_{0.84}\text{Ca}_{0.16}\text{O}_{1.84}$ , the conductivity increased with the decreasing of the grain size at temperatures below 800°C [16]. However, the transition of the  $\text{ZrO}_2$ -based solid electrolytes to the nanosized grain structure has not always increased the conductivity unambiguously. For instance,  $\text{ZrO}_2\text{--Y}_2\text{O}_3$ -samples with grains sized ~40 nm did not demonstrate any increase in their conductivity as compared with microcrystalline samples of similar composition [44]. Studies of the conductivity of micro- and nanostructured  $\text{ZrO}_2\text{--Y}_2\text{O}_3$  ceramics showed the conductivity of the grain boundaries to be by 2–3 orders of magnitude less than the conductivity of the crystal grain bulk

<sup>1</sup> Published based on the materials of the VII All-Russian Conference with International Participation “Fuel Cells and Power Plants Based on Them”, Chernogolovka, 2020.

[24–33, 38–40]. Correspondingly, the activation energy of the grain-boundary conductivity is ~1.0–1.2 eV, that is, higher than that of the grain conductivity (0.84–0.93 eV) [39, 40, 43].

The presence of impurities in the starting materials also affects the solid electrolyte transport characteristics. For example, the silica impurity decreased the zirconia intergrain conductivity significantly [24, 38, 40–43]. The addition of as small as 0.2 wt % of silica resulted in the decrease of the  $\text{ZrO}_2\text{--Y}_2\text{O}_3$  intergrain conductivity by a factor of 15 [43]. The addition of small amount of  $\text{Al}_2\text{O}_3$  increased the  $\text{ZrO}_2\text{--Y}_2\text{O}_3$  intergrain conductivity, however, it can decrease the grain bulk conductivity [45].

The high intergrain conductivity in the low-impurity ceramics can be explained by the presence of space charge and the lowering of the oxygen-vacancy and defect concentration at the grain boundaries [4, 24, 39, 40, 46–50].

At higher temperatures, the intercrystalline-boundary resistance differs but slightly from the grain bulk resistance; however, in the low-temperature region the difference becomes being significant. Therefore, the effect of the grain boundaries on the electrolyte ionic conductivity is of particular importance in the low-temperature applications.

Thus, the grain boundaries conductivity can be affected by the presence of impurities, the difference in the concentrations of the added impurities in grains and grain boundaries, the second phase segregation, the presence of space charge and microfissures, as well as combination of all these factors.

The zirconia-based materials can be also prepared by the melt crystallization in a cold crucible [17, 51, 52]. Unlike the ceramics, the single-crystal conductivity depends but on the melt initial composition and the crystallization conditions. The advantages of the method are: good processibility, rapid synthesis of solid solutions in the melt from the initial oxides, and the equipment allowing to obtain few hundred kilos of single crystals in a single technological cycle for 24 h. During the melting, a polycrystalline protective film is formed at walls and bottom of a split water-cooling tubular copper container. The film prevents the contact of the melt with the tubes; its composition is the same as that of the melt. Therefore, the single crystal nucleation is heterogeneous and multicentric. The design of the cold container does not provide for any special tools restricting the number of the grooving crystals (like those used in hot crucibles). The crystallization process produced an ingot comprised of columnar single crystals whose number and size depend on numerous parameters (the initial melt composition, the building and crystallization regime, etc.). The melting high temperatures (~3000°C) favor the melt purification from volatile impurities; the presence of the protective film favors its high purity because the melt is not contaminated by the material

of the “crucible.” In addition, in the course of the directional crystallization the crystals are purified from impurities, such as oxides of silicon, aluminum, titanium, tungsten, molybdenum, etc., which are pushed toward the melt’s upper part [17, 51, 52]. However, the using of single-crystal materials as solid electrolytes in electrochemical devices is limited by the complicated forms of the sensors and large size of electrolytical membranes. Although the problem can be solved in principle, yet, nowadays the mechanical processing of single crystals is rather expensive, and this restricts their application significantly.

In this work, we aimed at the determining of the effect of the stabilizing oxide ( $\text{Y}_2\text{O}_3$ ) concentration on the transport characteristics of the  $\text{ZrO}_2$ -based single-crystal solid solutions. Other goals are: the preparation of ceramic solid electrolytes by using a powder obtained from the molten material as a source material; the comparative analysis of structure and electro-physical properties of single-crystal and ceramic samples of the solid electrolytes.

## EXPERIMENTAL

The  $(\text{ZrO}_2)_{1-x}(\text{Y}_2\text{O}_3)_x$  ( $x = 0.08\text{--}0.12$ ) solid-solution single crystals were synthesized by directional crystallization of a melt in cold container. The parent stock were ultra-high purity grade oxides (assay no less than 99.96 wt %). The initial zirconium and yttrium oxides were mixed mechanically, charged into water-cooled tubular container, and melted by using direct microwave heating. The power generator frequency was 5.28 MHz; the power, 60 kW. Zirconium metal was used in the starting melting. The melt crystallization in the cold container produced an ingot comprising separate single crystals.

Some part of the crystals was crushed, the obtained powder was used as a parent stock in the manufacturing of ceramic samples. The crushing was carried out in a barrel lined with stabilized zirconia; the grinding bodies were made of the same material. To prepare the ceramics, we used the powder of particles sized 40  $\mu\text{m}$  with specific surface area about 8000  $\text{cm}^2/\text{g}$ . The ceramic samples were obtained by slip casting onto a moving substrate, by using an original setup manufactured at the EKON Enterprise. From the obtained film, raw parts of preset dimensions were cut off. The raw parts were annealed in air at a temperature of 1680°C for 2 h.

The ceramic and single-crystal sample phase composition was analyzed by X-ray diffraction analysis at a Bruker D8 diffractometer with  $\text{CuK}\alpha$ -radiation, as well as Raman spectroscopy, by using a laser with the wavelength of 633 nm as an excitation source. The density was determined by hydrostatic weighing using a Sartorius instrument. The samples’ microstructure was studied with a JEOL 5910 LV scanning electron

**Table 1.** Phase composition and crystal structure parameters of  $\text{ZrO}_2\text{--Y}_2\text{O}_3$  crystals

Sample	Phase composition*		Space group of symmetry	Lattice parameters, Å
	crystals	powders		
8YSZ	c	c	<i>Fm3m</i>	$a = 5.138 \pm 0.001$
		t	<i>P4<sub>2</sub>/nmc</i>	$a = 3.633 \pm 0.002$ $c = 5.143 \pm 0.002$
9YSZ	c	c	<i>Fm3m</i>	$a = 5.141 \pm 0.001$
10YSZ	c	c	<i>Fm3m</i>	$a = 5.144 \pm 0.001$
11YSZ	c	c	<i>Fm3m</i>	$a = 5.147 \pm 0.001$
12YSZ	c	c	<i>Fm3m</i>	$a = 5.149 \pm 0.001$

\* c means the cubic modification of  $\text{ZrO}_2$ ; t, the tetragonal modification of  $\text{ZrO}_2$ .

microscope equipped with an INCA-Energy energy-dispersive adapter.

The ceramic and single-crystal samples' conductivity was measured over a 300–900°C temperature range by using a Solartron SI 1260 frequency analyzer over a 1 Hz–5 MHz frequency range, applying an ac signal with amplitude of 24 mV. In the measurements, plane plate electrodes sized  $7 \times 7 \text{ mm}^2$  with a thickness of 0.5 mm were used. To make current contacts, platinum paste was applied to the crystals' opposing sides; it was burned-in in air at a temperature of 950°C for 1 h. The impedance spectra were processed using a ZView program (ver. 2.8). The crystals' conductivity was calculated from the results of the processing the impedance spectra, with taking into consideration the samples' geometrical dimensions.

## RESULTS AND DISCUSSION

In what follows, the  $\text{ZrO}_2$  single crystals grown by the directional crystallization in cold container and stabilized with 8, 9, 10, 11, and 12 mol %  $\text{Y}_2\text{O}_3$  are denoted as 8YSZ, 9YSZ, 10YSZ, 11YSZ, and 12YSZ, respectively. All crystals were transparent; they were columnar, what is characteristic of zirconia crystals obtained by the above-described method.

The crystals' phase composition is given in Table 1. To evaluate the crystals' phase resistance against mechanical action, the phase composition analysis was carried out both at the crystals and powders prepared therefrom.

All studied single crystals of the  $\text{ZrO}_2\text{--Y}_2\text{O}_3$  solid solutions had fluorite-type cubic structure. The studying of the phase composition of the powders prepared from the crystals showed that upon the grinding of the crystals their phase composition did not change, the sample 8YSZ being an exclusion. The powder prepared from the 8YSZ crystals comprised a mixture of the  $\text{ZrO}_2$  cubic and tetragonal modifications. Thus, the  $\text{ZrO}_2$  doping with 8 mol %  $\text{Y}_2\text{O}_3$  allowed stabilizing the high-temperature cubic structure in the solid solution; however, the cubic modification in the crystals is

nonstable and can exert a cubic-to-tetragonal phase transition upon the mechanical action.

The crystal phase composition was also analyzed by the Raman spectroscopy. In Fig. 1 we show the Raman spectra of the crystals.

In the Raman spectra of the 11YSZ and 12YSZ crystals we have lines characteristic of the cubic structure only. In the Raman spectra of the 8YSZ, 9YSZ, and 10YSZ crystals, in addition to the cubic-phase lines, a line at  $\sim 480 \text{ cm}^{-1}$  is present, which is characteristic of the tetragonal t"-phase [53–57]. This phase has the tetragonality degree  $c/\sqrt{2a} = 1$ , yet, it is classified as the *P4<sub>2</sub>/nmc* space group of symmetry because of the oxygen ion shift in the anion sublattice [54]. Thus, the 8YSZ, 9YSZ, and 10YSZ crystals are pseudocubic, they have the t"-phase structure.

In Fig. 2 we show temperature dependences of the conductivity for the  $\text{ZrO}_2\text{--Y}_2\text{O}_3$  crystals and the dependence of the solid solution conductivity on the  $\text{Y}_2\text{O}_3$  concentration at 1173 K.

Of the entire set of studied compositions, the 9YSZ crystals had the maximal conductivity over the entire temperature range. It follows from the data given in

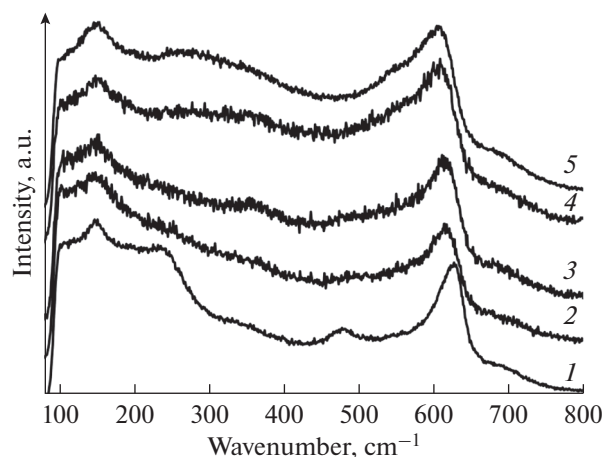


**Fig. 1.** Raman spectra of 8YSZ (1), 9YSZ (2), 10YSZ (3), 11YSZ (4), and 12YSZ (5) crystals.

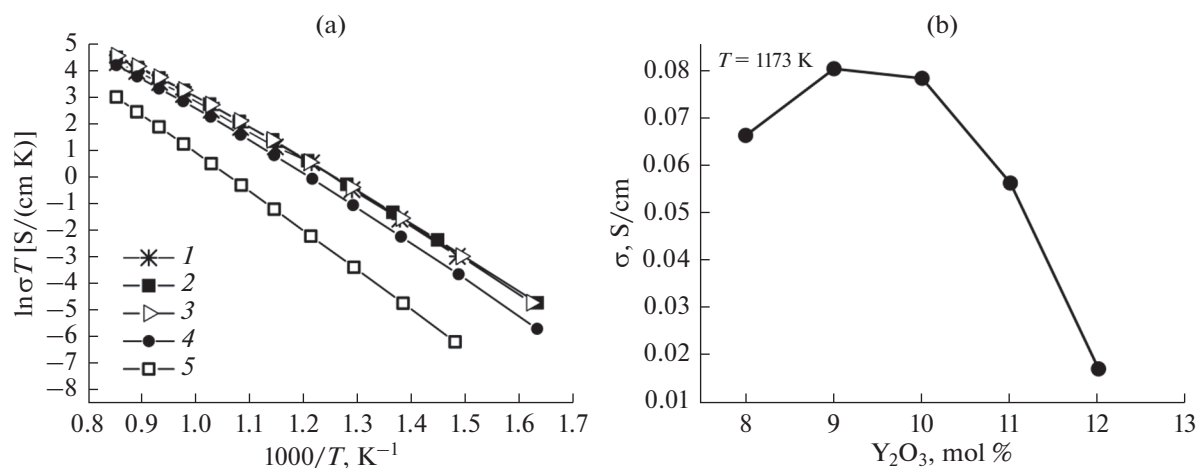


**Fig. 2.** Temperature dependence of conductivity (a) of 8YSZ (1), 9YSZ (2), 10YSZ (3), 11YSZ (4), and 12YSZ crystals (5) and dependence of the solid solutions' conductivity on the  $Y_2O_3$  concentration at 1173 K (b).

Fig. 2b that with the increasing of the  $Y_2O_3$  concentration the conductivity change is non-monotonic. With the increasing of the  $Y_2O_3$  concentration from 8 to 9 mol % the conductivity increased, and a weakly pronounced conductivity maximum is observed for the 9YSZ crystal. Further increasing of the  $Y_2O_3$  concentration up to 10 mol % influenced the conductivity but insignificantly. However, at further increase in the  $Y_2O_3$  concentration the solid solution conductivity decreased.

In the preparation of ceramic samples, we chose of the entire set of studied compositions the crystals containing 9 mol %  $Y_2O_3$  as the source material, because they had the maximal conductivity.

In Fig. 3 we present microstructure of a 9YSZ ceramic sample obtained by the slip casting onto a moving substrate.

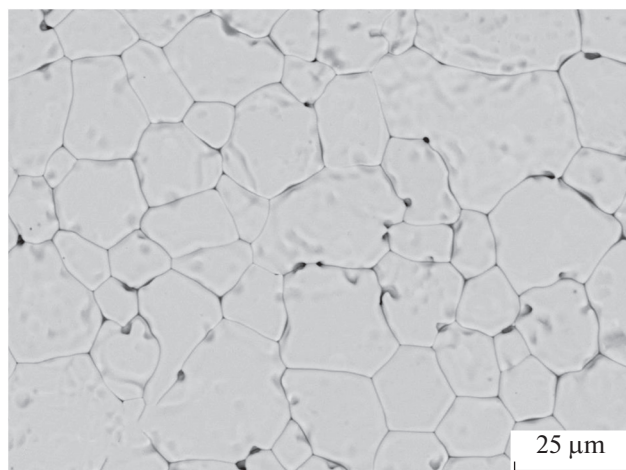


**Fig. 3.** The microstructure of the ceramic sample 9YSZ.

The density of the 9YSZ ceramic samples was  $\sim 5.86$  g/cm<sup>3</sup>. This value equals 98% of the density of poreless single crystals of the same composition ( $\sim 5.98$  g/cm<sup>3</sup>). The grain size in the samples varied from 10 to 30 μm. The energy-dispersive analysis detected alumina in the bulk and at grain boundaries. In Fig. 4 we present a microphotograph-image of separate grains in the 9YSZ sample, as well as the energy-dispersive analysis spectra in the grain bulk and at grain boundary. While in the grain bulk the  $Al_2O_3$  concentration did not exceed 0.5 mol %, in the grain boundaries the  $Al_2O_3$  concentration was significantly larger; at some spots, it was as large as 3 mol %.

The presence of the alumina in the ceramic samples is likely to be connected with the thermal treating of the raw parts after their slip casting, which was performed in closed alumina crucibles.

The alumina effect on the transport characteristics of the ceramic solid electrolytes was studied in works [58–62].  $Al_2O_3$  was shown to mainly accumulate at the grain boundaries because the  $Al_2O_3$  solubility in  $ZrO_2$  is very low.

According to the phase analysis, the manufacturing of the 9YSZ ceramic samples from crystals did not change the phase composition. In Fig. 5 we give Raman spectra of the single-crystal and polycrystalline 9YSZ sample. The Raman spectrum of the ceramic sample is close to that of the single-crystal one for the same composition. In the spectrum, the  $\sim 480$  cm<sup>-1</sup> line is present, which is characteristic of the pseudocubic structure of the  $t''$ -phase. According to the X-ray diffraction analysis data, the lattice parameter of the ceramic 9YSZ sample is less than that of the single crystal. This fact may be connected with the alumina building-in to the  $ZrO_2$ - $Y_2O_3$  solid solution.

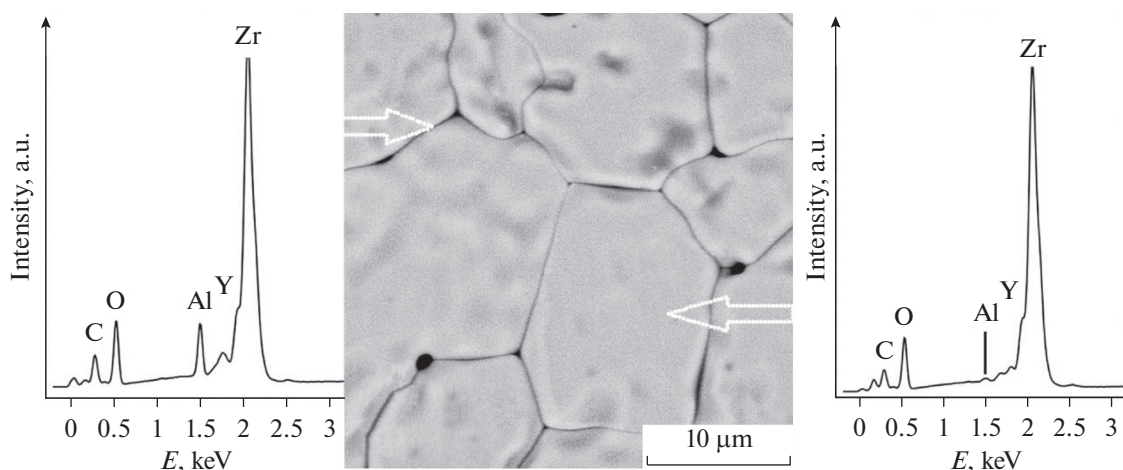


**Fig. 4.** Microphotograph of separate grains in the ceramic sample 9YSZ and the energy-dispersive analysis spectra taken in the grain bulk and at grain boundary.

To determine the bulk, grain-boundary, and full conductivities, we used the data derived from the processing of the impedance spectra. The crystals' bulk resistance ( $R_b$ ) was calculated in terms of the following model equivalent electrical circuit:  $(R_b - CPE_b)(R_{\text{electrode}} - CPE_{\text{electrode}})$  at lower temperatures (300–450°C); for the polycrystals, the bulk resistance was calculated in terms of the following equivalent electrical circuits:  $(R_b - CPE_b)(R_{\text{gb}} - CPE_{\text{gb}})(R_{\text{electrode}} - CPE_{\text{electrode}})$  and  $LR_b(R_{\text{electrode}} - CPE_{\text{electrode}})$  at higher temperatures (450–900°C) for the crystals and polycrystals, where  $R_{\text{electrode}}$  is the resistance of the electrode/electrolyte interface,  $CPE_{\text{electrode}}$  is the constant phase element characterizing processes at the electrode interface,  $R_{\text{gb}}$  is the resistance of grain boundaries,  $CPE_{\text{gb}}$  is the constant phase element characterizing processes at the grain boundaries,  $L$  is the inductivity of the current leads.

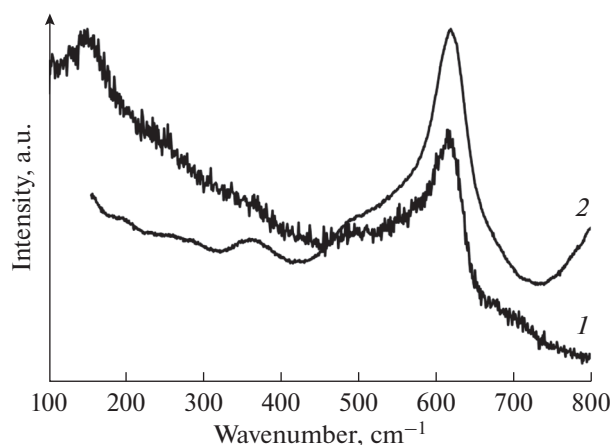


**Fig. 5.** Raman spectra of (1) single-crystal and (2) ceramic 9YSZ samples.

In Fig. 6 we show typical impedance spectra obtained at a temperature of 691 K for the 9YSZ single-crystal and ceramic samples.

The impedance spectra for the ceramic samples consist of three parts, well-separated at lower temperatures: the first high-frequency circumference presents the bulk resistance of the zirconia ceramics, the second circumference at moderate frequencies is connected with the resistance of the grains' inner boundaries, and the loop in the low-frequency region describes the electrode polarization resistance. In the impedance spectra for the polycrystals we see only two parts: a circumference in the high-frequency part of the spectrum, which describes the crystal bulk resistance, and the loop in the low-frequency region which describes the electrode polarization resistance.

The bulk conductivity ( $\sigma_b$ ) was determined by formula (1), the full conductivity ( $\sigma_{\text{total}}$ ) of ceramic sam-

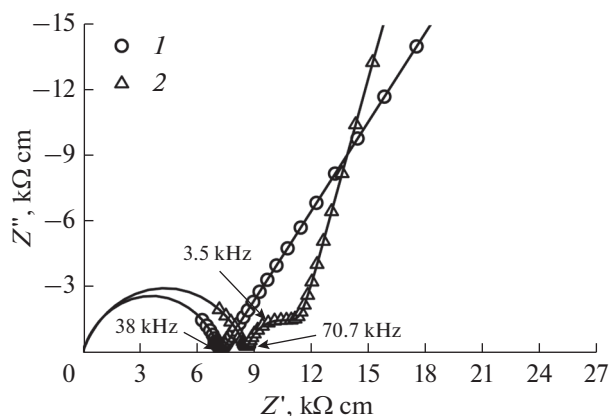


**Fig. 6.** Impedance spectra for (1) single-crystal and (2) ceramic samples of 9YSZ crystal at a temperature of 691 K.

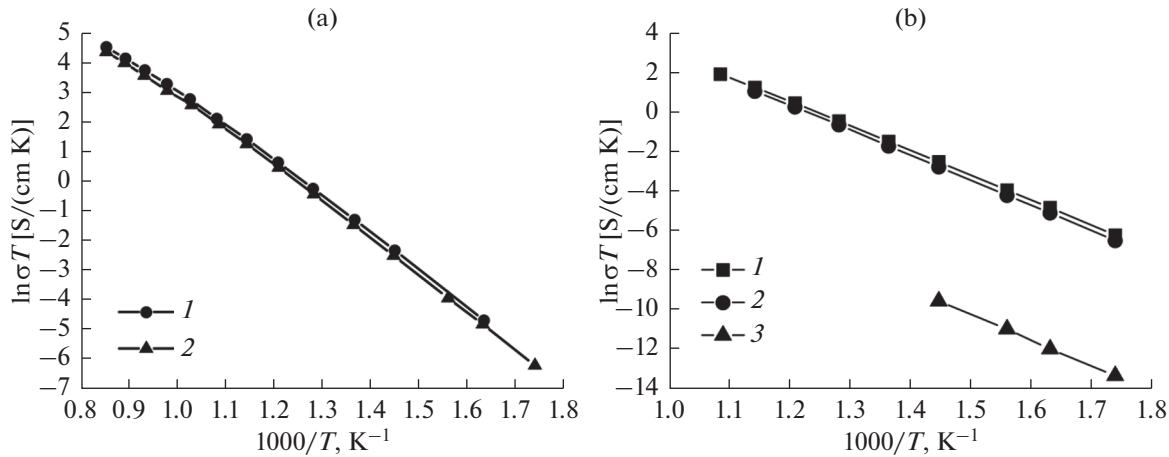


**Fig. 7.** Temperature dependences of conductivity of single-crystal (1) and ceramic (2) samples (a). Temperature dependences of the bulk (1), full (2), and grain-boundary (3) conductivities for the 9YSZ ceramic sample (b).

ples was calculated with the taking into consideration of the full resistance that is the sum of the bulk and grain-boundary resistances [10]:

$$\sigma_b = \frac{l}{R_b A}, \quad (1)$$

where  $l$  is the sample thickness,  $A$  is its surface area.

The grain-boundary conductivity ( $\sigma_{gb}$ ) for the ceramics was calculated by the following equation [10]:

$$\sigma_{gb} = \frac{C_b}{C_{gb}} \frac{l}{R_{gb} A}, \quad (2)$$

where  $C_b$  and  $C_{gb}$  is the bulk and grain-boundary capacitances, respectively; at that, we assumed that the grains and grain boundaries have similar dielectric constants [59]. To calculate the  $C_b$  and  $C_{gb}$  parameters, for each circuit we used the following formula [61]:

$$C = (R^{1-\alpha} Q)^\frac{1}{\alpha}, \quad (3)$$

where  $Q$  is the proportionality factor,  $\alpha$  is the exponent denoting the phase deviation.

In Fig. 7 we give temperature dependences for the bulk conductivity of the single-crystal and ceramic samples and those of the bulk, grain-boundary, and full conductivities for the ceramic sample, plotted in the Arrhenius coordinates.

For all studied ceramic samples, the grain conductivity was much larger (by a factor of  $\sim 10^3$ ) than that of grain boundaries at temperatures from 575 to 690 K, which is in compliance with the difference between the conductivities of grains and grain boundaries in the 8YSZ ceramics reported in work [10].

Data of different works [10, 23, 24, 39, 40] show the grain-boundary resistivity often being few orders of magnitude larger than the bulk resistivity. The grain boundaries in  $ZrO_2$  demonstrate blocking effect with

respect to ionic transport therethrough. The charge carrier transfer through the grain boundaries occurs only through intergrain contacts whose properties are determined by the space charge layer. The blocking effect is an inner phenomenon in itself; it occurs only in high-purity materials. A model was suggested [40] for defect structure of the grain boundaries in doped  $ZrO_2$ , in which a depletion in oxygen vacancies and enrichment with dopant in the space charge layer has been assumed. For the high-purity  $ZrO_2$ -based materials, the grain-boundary resistivity was shown being by 2–3 orders of magnitude larger than the grain bulk resistivity because of the blocking effect of the space-charge layer depleted in the oxygen vacancies. The activation energy of the grain-boundary resistivity is determined by the properties of the space-charge layer. The blocking effect is better pronounced at lower temperatures.

In the 9YSZ ceramic samples, the material's full conductivity decreased because of the increasing grain boundary resistivity. The ceramics' full conductivity over the 600–700 K temperature range ( $1 \times 10^{-5} - 1 \times 10^{-4}$  S/cm) is by a factor of 1.5 lower than that of single crystals ( $1.5 \times 10^{-5} - 1.4 \times 10^{-4}$  S/cm). With the increasing of temperature, the difference in the conductivity of crystals and ceramics made of molten material decreased because of decrease in the influence of the grain boundaries on the material's conductivity [24]. It is to be noted that in the 973–1173 K temperature range the ionic conductivities in single crystals and the ceramics made of molten material approach each other. In particular, at a temperature of 1173 K the single crystal conductivity is 0.086 S/cm, that of the ceramics is somewhat lower: 0.065 S/cm. The decrease in the grain bulk conductivity as compared with that of single crystals can be caused by the entry of small amount of alumina into the solid solution composition. The entry of alumina was reported

[53] to always lower the zirconia-based solid solution conductivity. This is due to the increase in the number of complexes of the  $\text{Al}^{3+}$  three-valent cations with oxygen vacancies and decrease in the concentration of free oxygen vacancies that are the charge carriers in the ionic conductance. The defect-complex formation upon the adding of  $\text{Al}_2\text{O}_3$  results in the decrease of the bulk-conductivity activation energy. In particular, the activation energy of the crystal and ceramics' conductivity was practically the same over the 973–1173 K temperature range: 0.87 eV. Over the 600–750 K temperature range, the activation energy of the single crystal conductivity was 1.07 eV; for the grain-boundary conductivity, 1.24 eV.

### CONCLUSIONS

Single crystals of the  $(\text{ZrO}_2)_{1-x}(\text{Y}_2\text{O}_3)_x$  ( $x = 0.08$ – $0.12$ ) solid-solutions were synthesized by directional crystallization of a melt. The effect of the  $\text{Y}_2\text{O}_3$  stabilizing oxide concentration on the transport characteristics and phase composition of the  $\text{ZrO}_2$ -based single-crystal solid solutions is studied. In the studied composition diapason, at the stabilizing oxide ( $\text{Y}_2\text{O}_3$ ) concentration  $\leq 10$  mol % the crystals were shown to have a pseudocubic  $t''$ -phase structure. At the  $\text{Y}_2\text{O}_3$  concentration  $> 10$  mol %, the crystals have a cubic fluorite-like structure. According to X-ray diffraction analysis, the  $(\text{ZrO}_2)_{0.92}(\text{Y}_2\text{O}_3)_{0.08}$  crystals have unstable phase composition; upon the mechanical action, tetragonal phase is formed in the materials.

The  $(\text{ZrO}_2)_{0.91}(\text{Y}_2\text{O}_3)_{0.09}$  crystals were shown to have the maximal conductivity. The crystals of this composition were crushed, the obtained powder was used as the parent stock in the manufacturing of ceramic samples by slip casting onto a moving substrate. The density of the  $(\text{ZrO}_2)_{0.91}(\text{Y}_2\text{O}_3)_{0.09}$  ceramic samples was 98% of the density of single crystals. The grain size in the prepared samples varied from 10 to 30  $\mu\text{m}$ . The energy-dispersive method detected the presence of alumina in the bulk and at grain boundaries.

A comparative analysis of structure and electro-physical properties of ceramic and single-crystal samples of the  $(\text{ZrO}_2)_{0.91}(\text{Y}_2\text{O}_3)_{0.09}$  solid electrolytes is carried out. The described method of the ceramic samples' preparation is shown not lead to changes in the phase composition and crystal structure of the ceramics. The ionic conductivity of the single crystals and ceramics prepared from molten material in the 973–1173 K temperature range approached each other; at a temperature of 1173 K, their conductivity values are 0.076 and 0.065 S/cm, respectively.

### FUNDING

This work was supported by the Russian Science Foundation, grant no. 19-72-10113. The structure study was carried out with the equipment of the Common Use Center

“Material Science and Metallurgy”; it obtained a financial support from the Ministry of Education and Science of Russian Federation (grant no. 075-15-2021-696).

### CONFLICT OF INTEREST

The authors declare that they have no conflict of interest.

### REFERENCES

1. Goodenough, J.B., Oxide-ion electrolytes, *Annu. Rev. Mater. Res.*, 2003, vol. 33, p. 91.
2. Kharton, V.V., Marques, F.M.B., and Atkinson, A., Transport properties of solid oxide electrolyte ceramics: A brief review, *Solid State Ionics*, 2004, vol. 174, p. 135.
3. Kilner, J.A. and Steele, B.C.H., *Nonstoichiometric Oxides*, New York.: Academic, 1981. p. 233.
4. Yamamoto, O., Solid oxide fuel cells: fundamental aspects and prospects, *Electrochim. Acta*, 2000, vol. 45, nos. 15–16, p. 2423.
5. Wachsman, E.D. and Lee, K.T., Lowering the temperature of solid oxide fuel cells, *Science*, 2011, vol. 334, p. 935.
6. Han, F., Mücke, R., Gestel, T.V., Leonide, A., Menzler, N.H., Buchkremer, H.P., and Stöver, D., Novel high-performance solid oxide fuel cells with bulk ionic conductance dominated thin-film electrolytes, *J. Power Sources*, 2012, vol. 218, p. 157.
7. Omar, S., Belda, A., Escardino, A., and Bonanos, N., Ionic conductivity ageing investigation of 1Ce10ScSZ in different partial pressures of oxygen, *Solid State Ionics*, 2010, vol. 184, p. 2.
8. Jasper, A., Kilner, J.A., and McComb, D.W., TEM and impedance spectroscopy of doped ceria electrolytes, *Solid State Ionics*, 2008, vol. 179, nos. 21–26, p. 904.
9. Jais, A.A., Ali, S.A.M., Anwar, M., Somalu, M.R., Muchtar, A., Isahak, W.N.R.W., Tan, C.Y., Singh, R., and Brandon, N.P., Enhanced ionic conductivity of scandia-ceria-stabilized-zirconia (10Sc1CeSZ) electrolyte synthesized by the microwave-assisted glycine nitrate process, *Ceram. International*, 2017, vol. 43, no. 11, p. 8119.
10. Zhang, J., Lenser, C., Menzler, N.H., and Guillon, O., Comparison of solid oxide fuel cell (SOFC) electrolyte materials for operation at 500°C, *Solid State Ionics*, 2020, vol. 344, p. 115138.
11. Yeh, T.-H., Hsu, W.-C., and Chou, C.-C., Mechanical and electrical properties of  $\text{ZrO}_2$  (3Y) doped with  $\text{RENbO}_4$  (RE = Yb, Er, Y, Dy, YNd, Sm, Nd), *J. Phys. IV France*, 2005, vol. 128, p. 213.
12. Kumar, A., Jaiswa, A., Sanbui, M., and Omar, S., Oxygen-ion conduction in scandia-stabilized zirconia-ceria solid electrolyte  $(x\text{Sc}_2\text{O}_3-1\text{CeO}_2-(99-x)\text{ZrO}_2, 5 \leq x \leq 11)$ , *J. Amer. Ceram. Soc.*, 2016, vol. 100, p. 659.
13. Lee, D.-S., Kim, W.S., Choi, S.H., Kim, J., Lee, H.-W., and Lee, J.-H., Characterization of  $\text{ZrO}_2$  co-doped with  $\text{Sc}_2\text{O}_3$  and  $\text{CeO}_2$  electrolyte for the application of intermediate temperature SOFCs, *Solid State Ionics*, 2005, vol. 176, nos. 1–2, p. 33.

14. Chen, X.J., Khor, K.A., Chan, S.H., and Yu, L.G., Influence of microstructure on the ionic conductivity of yttria-stabilized zirconia electrolyte, *Mater. Sci. Eng.: A*, 2002, vol. 335, nos. 1–2, p. 246.
15. Abbas, H.A., Argirusis, C., Kilo, M., Wiemhöfer, H.-D., Hammad, F.F., and Hanafi, Z.M., Preparation and conductivity of ternary scandia-stabilised zirconia, *Solid State Ionics*, 2011, vol. 184, no. 1, p. 6.
16. Tien, T.Y., Grain boundary conductivity of  $Zr_{0.84}Ca_{0.16}O_{1.84}$  ceramics, *J. Appl. Phys.*, 1964, vol. 35, p. 122.
17. Osiko, V.V., Borik, M.A., and Lomonova, E.E., *Handbook of Crystal Growth*, Berlin: Springer, 2010, p. 433–469.
18. Spirin, A., Ivanov, V., Nikonov, A., Lipilin, A., Parandin, S., Khrustov, V., and Spirina, A., Scandia-stabilized zirconia doped with yttria: synthesis, properties, and ageing behavior, *Solid State Ionics*, 2012, vol. 225, p. 448.
19. Omar, S., Najib, W.B., Chen, W., and Bonanos, N., Electrical conductivity of 10 mol %  $Sc_2O_3$ –1 mol %  $M_2O_3$ – $ZrO_2$  ceramics, *J. Amer. Ceram. Soc.*, 2012, vol. 95, no. 6, p. 1965.
20. Rocha, R.A., Muccillo, E.N.S., Dessemonda, L., and Djurado, E., Thermal ageing of nanostructured tetragonal zirconia ceramics: characterization of interfaces, *J. Europ. Ceram. Soc.*, 2010, vol. 30, p. 227.
21. Araki, W., Koshikawa, T., Yamaji, A., and Adachi, T., Degradation mechanism of scandia-stabilised zirconia electrolytes: discussion based on annealing effects on mechanical strength, ionic conductivity, and Raman spectrum, *Solid State Ionics*, 2009, vol. 180, nos. 28–31, p. 1484.
22. Hirano, M., Watanabe, S., Kato, E., Mizutani, Y., Kawai, M., and Nakamura, Y., High electrical conductivity and high fracture strength of  $Sc_2O_3$ -doped zirconia ceramics with submicrometer grains, *J. Amer. Ceram. Soc.*, 1999, vol. 82, no. 10, p. 2861.
23. Irvine, J.T.S., Sinclair, D.C., and West, A.R., Electroceramics: Characterization by impedance spectroscopy, *Adv. Mater.*, 1990, vol. 2, no. 3, p. 132.
24. Hui, S.R., Roller, J., Yick, S., Zhang, X., Decés-Petit, C., Xie, Y., Maric, R., and Ghosh, D., A brief review of the ionic conductivity enhancement for selected oxide electrolytes, *J. Power Sources*, 2007, vol. 172, no. 2, p. 493.
25. Kilo, M., Taylor, M.A., Argirusis, C., Borchardt, G., Lesage, B., Weber, S., Scherrer, S., Scherrer, H., Schroeder, M., and Martin, M., Cation self-diffusion of  $^{44}Ca$ ,  $^{88}Y$  and  $^{96}Zr$  in single crystalline calcia- and yttria-doped zirconia, *J. Appl. Phys.*, 2003, vol. 94, no. 12, p. 7547.
26. Chevalier, J., Gremillard, L., Virkar, A.V., and Clarke, D.R., The tetragonal-monoclinic transformation in zirconia: lessons learned and future trends, *J. Amer. Ceram. Soc.*, 2009, vol. 92, no. 9, p. 1901.
27. Aktas, B., Tekeli, S., and Kucuktuvek, M., Electrical conductivity of  $Er_2O_3$ -doped c- $ZrO_2$  ceramics, *J. Mater. Eng. Perform.*, 2014, vol. 23, no. 1, p. 349.
28. Cheikh, A., Madani, A., Touati, A., Boussetta, H., and Monty, C., Ionic conductivity of zirconia based ceramics from single crystals to nanostructured polycrystals, *J. Europ. Ceram. Soc.*, 2001, vol. 21, nos. 10–11, p. 1837.
29. Aoki, M., Chiang, Y.-M., Kosacki, I., Lee, L.J.-R., Tuller, H., and Liu, Y., Solute segregation and grain-boundary impedance in high-purity stabilized zirconia, *J. Amer. Ceram. Soc.*, 1996, vol. 79, no. 5, p. 1169.
30. Shukla, S., Seal, S., Vij, R., and Bandyopadhyay, S., Reduced activation energy for grain growth in nanocrystalline yttria-stabilized zirconia, *Nano Letters*, 2003, vol. 3, no. 3, p. 397.
31. Mondal, P., Klein, A., Jaegermann, W., and Hahn, H., Enhanced specific grain boundary conductivity in nanocrystalline  $Y_2O_3$ -stabilized zirconia, *Solid State Ionics*, 1999, vol. 118, nos. 3–4, p. 331.
32. Choen, K.-W., Chen, J., and Xu, R., Metal–organic vapor deposition of YSZ electrolyte layers for solid oxide fuel cell applications, *Thin Solid Films*, 1997, vol. 304, no. 1–2, p. 106.
33. Liaw, B.Y. and Weppner, W., Low temperature limiting-current oxygen sensors based on tetragonal zirconia polycrystals, *J. Electrochem. Soc.*, 1991, vol. 138, no. 8, p. 2478.
34. Brett, D.J.L., Atkinson, A., Brandon, N.P., and Skinner, S.J., Intermediate temperature solid oxide fuel cells, *Chem. Soc. Rev.*, 2008, vol. 37, p. 1568.
35. Badwal, S.P.S. and Drennan, J., The effect of thermal history on the grain boundary resistivity of Y-TZP materials, *Solid State Ionics*, 1988, vol. 28–30, p. 1451.
36. Ye, F., Mori, T., Ou, D.R., Takahashi, M., Zou, J., and Drennan, J., Ionic conductivities and microstructures of ytterbium-doped ceria, *J. Electrochem. Soc.*, 20007, vol. 154, no. 2, p. B180.
37. Gerhardt, R. and Nowick, A.S., Grain boundary effect in ceria doped with trivalent cations: I, Electrical measurements, *J. Amer. Ceram. Soc.*, 1986, vol. 69, no. 9, p. 641.
38. Wang, D.Y. and Nowick, A.S., The “grain-boundary effect” in doped ceria solid electrolytes, *J. Solid State Chem.*, 1980, vol. 35, no. 3, p. 325.
39. Guo, X. and Waser, R., Electrical properties of the grain boundaries of oxygen ion conductors: Acceptor-doped zirconia and ceria, *Prog. Mater. Sci.*, 2006, vol. 51, p. 151.
40. Guo, X. and Maier, J., Grain boundary blocking effect in zirconia: a Schottky barrier analysis, *J. Electrochem. Soc.*, 2001, vol. 148, no. 3, p. E121.
41. Tuller, H.L., Ionic conduction in nanocrystalline materials, *Solid State Ionics*, 2000, vol. 131, nos. 1–2, p. 143.
42. Heitjans, P. and Indris, S., Diffusion and ionic conduction in nanocrystalline ceramics, *J. Phys: Condens. Matter*, 2013, vol. 15, no. 30, p. R1257.
43. Badwal, S.P.S., Grain boundary resistivity in zirconia-based materials: effect of sintering temperatures and impurities, *Solid State Ionics*, 1995, vol. 76, nos. 1–2, p. 67.
44. Mondal, P. and Hahn, H., Investigation of the complex conductivity of nanocrystalline  $Y_2O_3$ -stabilized zirconia, *Ber. Bunsenges. Phys. Chem.*, 1997, vol. 101, no. 11, p. 1765.

45. Lee, J.-H., Mori, T., Li, J.-G., Ikegami, T., Komatsu, M., and Haneda, H., Improvement of grain-boundary conductivity of 8 mol % yttria-stabilized zirconia by precursor scavenging of siliceous phase, *J. Electrochem. Soc.*, 2000, vol. 147, no. 7, p. 2822.
46. Maier, J., Space charge regions in solid two phase systems and their conduction contribution – II contact equilibrium at the interface of two ionic conductors and the related conductivity effect, *Ber. Bunsenges. Phys. Chem.*, 1985, vol. 89, no. 4, p. 355.
47. Guo, X., Sigle, W., Fleig, J., and Maier, J., Role of space charge in the grain boundary blocking effect in doped zirconia, *Solid State Ionics*, 2002, vol. 154–155, p. 555.
48. Liu, T., Zhang, X., Wang, X., Yu, J., and Li, L., A review of zirconia-based solid electrolytes, *Ionics*, 2016, vol. 22, p. 2249.
49. Röwer, R., Knöner, G., Reimann, K., Schaefer, H.-E., and Södervall, U., Oxygen diffusion in YSZ single crystals at relatively low temperatures, *Phys. Stat. Sol. B*, 2003, vol. 239, no. 2, p. R1.
50. Badwal, S.P.S. and Rajendran, S., Effect of micro- and nano-structures on the properties of ionic conductors, *Solid State Ionics*, 1994, vol. 70–71, p. 83.
51. Lomonova, E.E. and Osiko, V.V., *Growth of Zirconia Crystal by Skull-Melting Technique*, in *Crystal Growth Technology*, Scheel, H.J. and Fukuda, T., eds., New York: Wiley, 2003, p. 461–486.
52. Kuz'minov, Yu.S., Lomonova, E.E., and Osiko, V.V., *Cubic Zirconia and Skull Melting*, Cambridge: Cambr. Internat. Sci. Publ., 2009.
53. Yashima, M., Sasaki, S., Kakihana, M., Yamaguchi, Y., Arashi, H., and Yoshimura, M., Oxygen-induced structural change of the tetragonal phase around the tetragonal-cubic phase boundary in  $ZrO_2$ - $YO_{1.5}$  solid solutions, *Acta Crystallogr. B Struct. Sci.*, 1994, vol. B50, p. 663.
54. Yashima, M., Ohtake, K., Kakihana, M., Arashi, H., and Yoshimura, M., Determination of tetragonal-cubic phase boundary of  $Zr_{1-x}R_xO_{2-x/2}$  (R = Nd, Sm, Y, Er and Yb) by Raman scattering, *J. Phys. Chem. Solids*, 1996, vol. 57, no. 1, p. 17.
55. Hemberger, Y., Wichtner, N., Berthold, C., and Nickel, K.G., Quantification of yttria in stabilized zirconia by Raman spectroscopy, *Int. J. Appl. Ceram. Technol.*, 2016, vol. 13, no. 1, p. 116.
56. Borik, M.A., Bredikhin, S.I., Bublik, V.T., Kulebyakin, A.V., Kuritsyna, I.E., Lomonova, E.E., Milovich, P.O., Myzina, V.A., Osiko, V.V., Ryabochkina, P.A., and Tabachkova, N.Y., Structure and conductivity of yttria and scandia-doped zirconia crystals grown by skull melting, *J. Amer. Ceram. Soc.*, 2017, vol. 100, no. 12, p. 5536.
57. Agarkov, D.A., Borik, M.A., Bredikhin, S.I., Burmistrov, I.N., Eliseeva, G.M., Kolotygin, V.A., Kulebyakin, A.V., Kuritsyna, I.E., Lomonova, E.E., Milovich, F.O., Myzina, V.A., Ryabochkina, P.A., Tabachkova, N.Yu., and Volkova, T.V., Structure and transport properties of zirconia crystals co-doped by scandia, ceria and yttria, *J. Materiomics*, 2019, vol. 5, no. 2, p. 273.
58. Guo, X., Roles of alumina in zirconia for functional applications, *J. Amer. Ceram. Soc.*, 2003, vol. 86, no. 11, p. 1867.
59. Miyayama, M., Yanagida, H., and Asada, A., Effects of  $Al_2O_3$  additions on resistivity and microstructure of yttria-stabilized zirconia, *J. Amer. Ceram. Soc. Bull.*, 1986, vol. 65, no. 4, p. 74.
60. Navarro, L.M., Recio, P., Jurado, J.R., and Duran, P., Preparation and properties evaluation of zirconia-based/ $Al_2O_3$  composites as electrolytes for solid oxide fuel cell systems, Part III, Mechanical and electrical characterization, *J. Mater. Sci.*, 1995, vol. 30, p. 1949.
61. Feighery, J. and Irvine, J.T.S., Effect of alumina additions upon electrical properties of 8 mol % yttria-stabilized zirconia, *Solid State Ionics*, 1999, vol. 121, p. 209.
62. Ross, I.M., Rainforth, W.M., McComb, D.W., Scott, A.J., and Brydson, R., The role of trace additions of alumina to yttria-tetragonal zirconia polycrystals (Y-TZP), *Scr. Mater.*, 2001, vol. 45, no. 6, p. 653.

Translated by Yu. Pleskov